Firing propagation in empirical cognitive networks of human brain

Dehua Chen, Ruohua Gao, Zhiyin Yang, Siyu Huo, and Zonghua Liu*
School of Physics and Electronic Science, East China Normal University, Shanghai 200062, People's Republic of China

(Received 1 August 2024; accepted 17 January 2025; published 30 January 2025)

Understanding the physical mechanisms of brain functions has always been a challenging problem in the fields of nonlinear dynamics and network science. A promising approach to address this problem is by studying signal propagation on brain cognitive networks. So far, in the context of signal propagation, some progress has been achieved on complex networks, especially on the *Caenorhabditis elegans* network, but little attention has been paid to the empirical cognitive networks of the human brain, which are the networks responsible for cognitive tasks. Here we study how neural firings are propagated in the empirical cognitive networks of human brain. We find that the firing propagation can be seriously influenced by both the global topology of the network and the local topology of the source node. There is an optimal range of coupling strength related to synchronization for each source node, and multiple source nodes favor firing propagation. Further, we show that peripheral nodes of a network may have stronger ability of firing propagation than hub nodes. Interestingly, a remote firing propagation is observed, where firings are not propagated in a sequential rule, but propagated to farther distant nodes without the firings of intermediate nodes. A detailed theoretical analysis is provided to explain both the firing propagation and remote firing propagation.

DOI: 10.1103/PhysRevResearch.7.013116

I. INTRODUCTION

The physical mechanisms of brain function have always been a hot topic of interest. So far, many dynamical models of brain activity in human brain networks and biophysically motivated large-scale brain models have been proposed; see reviews for details [1–6]. These studies have established that synchronization is closely related to brain functions. For example, neural correlates of visual awareness may be related to synchronous neural firing at gamma frequencies [7]. And epileptic seizures correspond to an abnormal synchronization spreading on the whole brain network [8]. Therefore, to understand the physical mechanisms of brain functions, much attention has been paid to various synchronizations, such as complete synchronization, phase synchronization, delay synchronization, generalized synchronization, and explosive synchronization [9–11]. Recently, chimera state and remote synchronization have become central topics in nonlinear dynamics and network science [12–15], as the former can be used to explain the mechanism of the unihemispheric sleep in aquatic animals and migrated birds [16–18], while the latter can help us understand how brain functional networks emerge from brain structural networks.

In principle, all kinds of synchronization are induced by different coupling modes. In a specific synchronization process, oscillators will influence each other by exchanging information. However, the detailed process of exchanging information is often challenging to study. As an alternative, researchers have investigated signal propagation [19–24]. This approach provides insights into how information propagates from one node to another. For weak signals, two notable effects have been revealed. The first is topological resonance, in which the heterogeneity of scale-free networks facilitates the detection of weak signals [19]. The second is coupling resonance, where mixed positive and negative couplings enhance the detection of signals [23]. Recently, a new perturbation method has been developed to track information propagation, effectively capturing the network's role in propagating local information [25–27].

An application of signal propagation is in the brain network where every individual brain function is performed by a specific cognitive network and its functioning is activated by a specific external signal [28], such as one of the signals of light, sound, taste, and smell. Since the brain neural network contains approximately 10^{11} neurons and 10^{14} links, it is too complicated to study in its entirety. For simplicity, some primary works have been done on the network of *Caenorhabditis elegans* [29], which contains information on 277 out of those 302 neurons [30,31]. Surprisingly, in addition to the normal firing propagation in a sequential rule, an abnormal firing propagation was revealed. It is named *remote firing propagation* (RFP) [32,33], being an abnormal firing propagation between two distant and indirectly connected nodes with the intermediate nodes inactivated. Its mechanism can be also investigated by a model of bistable oscillators [34]. Recently, this kind of remote response mode has been discussed on the paced excitable *C. elegans* network [35].

A feature of the *C. elegans* network is its directional links. This network has 2105 directional links, where only 187 links are bidirectional and all the other 1731 links are unidirectional [29]. Thus, unidirectional links are a majority. It was revealed

*Contact author: zhliu@phy.ecnu.edu.cn

that the existence of the unidirectional links is the key element to generating the local firing propagation. Also, the configuration of the unidirectional links will seriously influence the range of firing propagation [33]. Moreover, it was found that the unidirectional links favor RFP [32]. In fact, this kind of directional link is also the feature of human neural networks where the interaction between two neurons is from the axon of one neuron to the dendrite of another neuron. However, due to the large size and complicated topology, the human neural network is usually simplified into a brain network. In the simplified version, a node represents a region of interest (ROI), and a connection between two ROIs is derived from the number of fibers found by the tractography algorithm. In this sense, the brain network is undirected because current imaging methods are unable to resolve directions. Then an interesting question is how firings are propagated in bidirectional cognitive networks of human brain [36,37]. On the other hand, among all these previous studies of RFP, Ref. [34] is the only one that used real data of brain network. However, a deficiency of Ref. [34] is that it is on the whole brain network instead of each specific cognitive network where a specific external signal is detected. Individual cognitive networks are different from each other, with some of their differences more significant. Thus, it is also of interest to study how the topologies of these cognitive networks influence firing propagation and even RFP if it applies.

To figure out the answers, we take a closer look at realistic brain cognitive networks, i.e., the eight empirical cognitive networks of human brain, which are responsible for cognitive tasks. We study how firings are propagated on them. In particular, we represent the dynamics of each node with a neural model so that the threshold effect of neurons can be reflected, unlike the previous studies with no threshold effect of neurons [19–23,34]. We find that the firing propagation can be seriously influenced by both the global topology of network and local topology of source node. We also show that there is an optimal range of coupling strength for each source node and multiple source nodes favor firing propagation. Interestingly, we observe a RFP where firings are propagated to distant nodes, without the firings of intermediate nodes. Further, a detailed theoretical analysis is provided to explain both firing propagation and RFP.

II. THE MODEL OF FIRING PROPAGATION IN COGNITIVE NETWORKS OF HUMAN BRAIN

It is well known that each specific brain function is in fact performed by only one or a few cognitive networks but not the whole brain network [38–41]. Thus, we focus on the firing propagation in cognitive networks of human brain in this work. To study this problem, we have to first obtain the connection matrices of these cognitive networks. For this purpose, we here consider an empirical brain network from the data of Refs. [36,37], which is a weighted network with 998 nodes, i.e., region of interest (ROI), and 17 865 bidirectional connections among them [42]. Each connection between two ROIs was measured noninvasively by using diffusion spectrum imaging (DSI), and its weight was derived from the number of fibers found with the tractography algorithm. Due to resolution limitation of DSI, there are nine isolated nodes

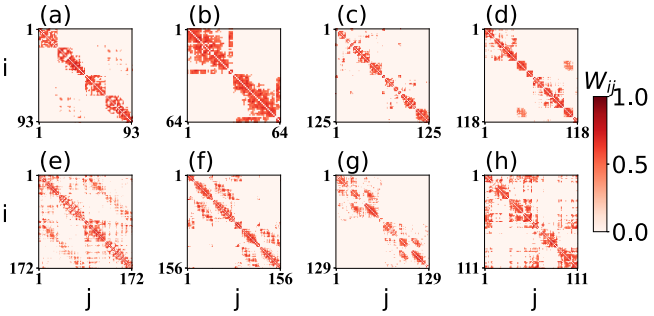

FIG. 1. The connection matrices of the eight cognitive networks extracted from the whole brain network where the color bar represents the weights W_{ij}. Panels (a)–(h) represent the weight matrices of the eight cognitive networks of Attention (Att), Auditory (Aud), Cingulo-opercular (CP), Frontoparietal (FP), Medial default mode (mDm), Motor and somatosensory (MS), Ventral temporal association (VT), and Visual (V) networks, respectively.

without detected fibers. To keep the connectivity of all the nodes, these nine isolated nodes were removed, leaving 989 nodes [42]. On the other hand, Ref. [43] shows an alternative approach to divide the cerebral cortex into 76 brain regions and then further divide them into nine cognitive networks. This framework of classification is mainly based on how the stimulation of different brain regions drives brain function and how brain function is constrained by variability in structural connectivity, i.e., each cognitive network represents the coactivated regions in support of a generalized class of cognitive functions. That is, these nine cognitive networks have clear functional roles and thus are named Attention (Att), Auditory (Aud), Cingulo-opercular (CP), Frontoparietal (FP), Medial default mode (mDm), Motor and somatosensory (MS), Ventral temporal association (VT), Visual (V), and Subcortical networks, respectively. For example, Aud, V, MS, and VT are sensory motor-related systems, Att and mDm are involved in functional roles that are generic across cognitive performance, CP and FP are associated with cognitive control, and the subcortical network consists of the regions responsible for autonomic and primal functions. In this study, we follow the framework of Ref. [43] to classify the brain network of 989 nodes. We find that each of the first eight cognitive networks is well connected, resulting in a total 968 nodes, while the remaining 21 nodes for the Subcortical network is not well connected. Thus, in this work, we consider only the first eight cognitive networks and exclude the Subcortical network. In each cognitive network, only the connections within the cognitive network are retained, while all connections between the eight cognitive networks are removed. Figures 1(a)–1(h) show the weighted connection matrices W_{ij} of the eight cognitive subnetworks, respectively. The weights of different cognitive networks have different distributions, but all of them can be approximated as Gaussian distributions around $W = 0.5$ [44].

A notable feature of Fig. 1 is that the connections in each of the eight cognitive networks are unevenly distributed, forming a topology of communities, in contrast to the random homogeneous networks and scale-free networks. We aim to understand how this feature influences their firing propagation. Additionally, the sizes N of these eight cognitive networks are different, ranging from 64 to 172, which may

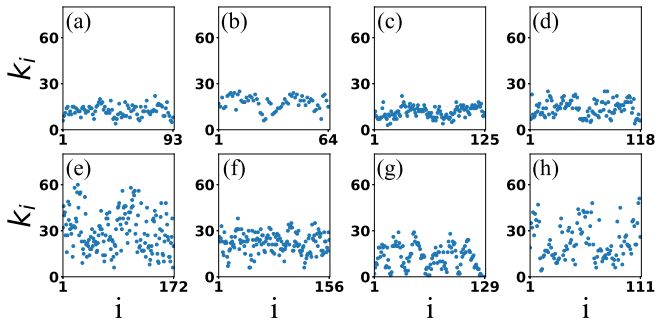

FIG. 2. Node degrees of cognitive networks where (a)–(h) represent the cases of the eight cognitive networks in Figs. 1(a)–1(h), respectively.

result in differing node degrees. Figures 2(a)–2(h) show the node degrees of the eight cognitive networks in Figs. 1(a)–1(h), respectively. Two features can be summarized from Fig. 2: (i) There is no positive correlation between their average degrees $\langle k\rangle$ and sizes N and (ii) the degree distributions are very dispersed in Figs. 2(e) and 2(h) but not so much in others. We also wonder how these two features influence their firing propagations.

To figure out the answers to these problems, the key is the choice of nodes dynamics of cognitive networks. Each node of brain network represents a ROI of cerebral cortex. The node dynamics are generally considered as a mean field of neurons in the ROI and can be represented by neuron mass models, such as the Wilson-Cowan model [45] and its variations [46–49]. These models describe network dynamics at the macroscopic level but cannot reflect the firings of neurons at the microscopic level. This creates a challenging situation where we lack both firing models of the macroscopic level and network topology of the vast number of neurons at the microscopic level. To solve this problem, we here assume that the macroscopic topology of brain network partially reserves the characteristic feature of the connectome of neurons, as the former can be considered as a renormalization of the latter [50]. In this sense, we here assume that the dynamics of each node can be described by the Hindmarsh-Rose (HR) model, which may have both bursting and spiking behaviors of neurons [51]. The HR model consists of three variables $x(t)$, $y(t)$, and $z(t)$, where x is the membrane potential, y is associated with the fast current Na^+ or K^+, and z corresponds to the slow current, for example, Ca^{2+}. The nodes dynamics can be represented by the following dynamical equations:

$$\begin{aligned}\frac{dx_i}{dt} &= y_i + bx_i^2 - ax_i^3 - z_i + I_{\rm ext} + \lambda\Sigma_{j=1}^{N} W_{ij}(x_j - x_i),\\ \frac{dy_i}{dt} &= c - dx_i^2 - y_i,\\ \frac{dz_i}{dt} &= r[e(x_i - x_0) - z_i],\end{aligned} \tag{1}$$

where i represents node i with $i \in [1, N]$, W_{ij} is one of the weighted matrices of Figs. 1(a)–1(h), $I_{\rm ext}$ is the external current input, λ is the coupling strength, and the parameters are taken as $a = 1.0$, $b = 3.0$, $c = 1.0$, $d = 5.0$, $r = 0.006$, $e = 4.0$, and $x_0 = -1.60$ [52].

Following Refs. [32,33], we set the external current $I_{\rm ext}$ to a value slightly smaller than the critical point of a single HR neuron, $I_{\rm ext}^c \approx 1.309$, so that the cognitive network is inactivated when there are no initial activated nodes; that is, we fix $I_{\rm ext} = 1.3 < I_{\rm ext}^c$ in this work. Then we will study how firings are propagated in different cognitive networks by choosing one or multiple nodes as the source nodes. For a chosen source node s, we give it a stimulus I_s so that the source node s will be activated when $\lambda = 0$. Therefore, for the source node s, the second and third equations of Eq. (1) will remain unchanged, but the first equation of Eq. (1) will be replaced by

$$\frac{dx_s}{dt} = y_s + bx_s^2 - ax_s^3 - z_s + I_{\rm ext} + I_s + \lambda\Sigma_{j=1}^{N} W_{sj}(x_j - x_s), \tag{2}$$

where the external stimulus I_s is fixed as $I_s = 1.7$ as in Refs. [32,33].

Equations (1) and (2) constitute our model of firing propagation on cognitive networks, which takes account of both the threshold effect of neurons and community topology of empirical cognitive brain networks.

III. NUMERICAL SIMULATIONS

In numerical simulations, we let the source nodes be represented by Eq. (2) and all the other nodes be represented by Eq. (1). In the following, we will discuss how firings are propagated in cognitive networks.

A. Firing propagation in cognitive networks of human brain with one source node

We first discuss the case of only one source node. As the HR model is a neural model, it will have two states, i.e., activated (firing) and inactivated. To check the status of nodes, we assume that there is a firing threshold as $x_c = 0$ [32,33]. A node i will be considered as activated or firing once its x_i variable reaches $x_i \geqslant x_c$, and inactivated, otherwise. In this way, we can check whether the firing of the source node is propagated to other nodes or not. We take the visual network as an example. Figure 3 shows two typical pathways of firing propagation from a source node for $\lambda = 0.1$, where the "red" and "gray" circles represent the firing nodes and inactivated nodes, respectively, and the source node is the node 80 with degree $k_{80} = 15$ in Fig. 3(a) and the node 11 with degree $k_{11} = 12$ in Fig. 3(b). The results show that the firing of the source node successfully propagates to other nodes in Fig. 3(a) but not in Fig. 3(b), suggesting that the firing propagation depends on the specific source nodes.

To measure the effect of firing propagation, we let $n_f(i)$ be the number of activated nodes in the whole cognitive network by the source node i. Then we measure how $n_f(i)$ depends on the source node i and the coupling strength λ. We first consider the case of visual network with $N = 111$. Figures 4(a) and 4(b) show the dependence of $n_f(i)$ on the chosen source node i and the coupling λ, respectively, with $\lambda = 0.1$ in Fig. 4(a) and the source node 80 in Fig. 4(b). We see from Fig. 4(a) that n_f can be either greater than zero for some nodes or zero for other nodes, corresponding to the two cases of Figs. 3(a) and 3(b), respectively. In particular, for the case of $n_f = 0$, most

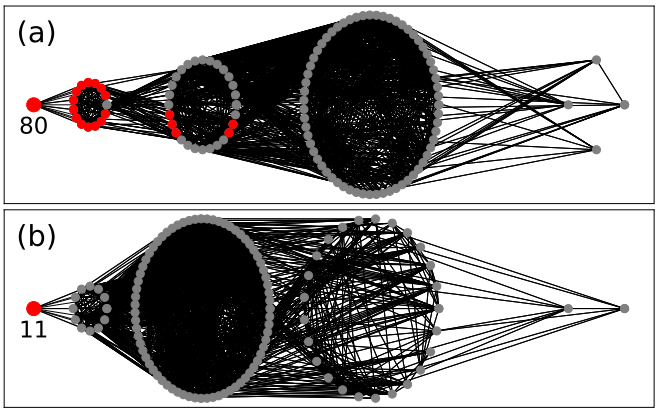

FIG. 3. Two typical pathways of firing propagation from a source node of the visual network, where the "red" and "gray" circles represent the firing nodes and inactivated nodes, respectively, with the coupling strength being fixed as $\lambda = 0.1$. Panels (a) and (b) represent the cases of successfully and unsuccessfully propagated firings from the source nodes to their nearest neighbors and so on, respectively, with the source node being node 80 in (a) and node 11 in (b).

of the source nodes are not even activated, as indicated by the "black" points along the x axis in Fig. 4(a). We will explain it in Sec. IV. Figure 4(b) shows that n_f is greater than zero when $0.02 < \lambda < 0.2$ and zero otherwise, implying that firing can be propagated only within an optimal coupling range; that is, too large or too small coupling will prevent firing propagation. Additionally, Fig. 4(c) shows the phase diagram of n_f on the phase plane of the source node i and the coupling strength λ. We see that n_f is greater than zero only in two regions. Therefore, a successful firing propagation depends on both the local topology of the source node i and the coupling strength λ.

Second, we consider the case of ventral network with $N = 129$. We observe similar results to those seen in the case of the

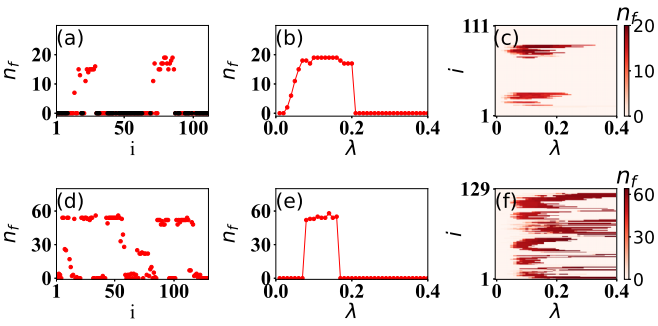

FIG. 4. Dependence of firing propagation on the source node i and the coupling strength λ. Panels (a)–(c) represent the case of a visual network, where (a) represents the dependence of the number of activated nodes n_f on the source node i, and the "black" points on the x axis denote the inactivated source nodes, with the coupling strength $\lambda = 0.1$; (b) shows the dependence of n_f on λ for the source node 80; and (c) represents the phase diagram of n_f on both the source node i and the coupling strength λ, with the color bar being the number n_f. Panels (d)–(f) represent the case of a ventral network, where (d) represents the dependence of n_f on the source node i, with the coupling strength $\lambda = 0.1$; (e) shows the dependence of n_f on λ for the source node 24; and (f) represents the phase diagram of n_f on both the source node i and the coupling strength λ, with the color bar being the number n_f.

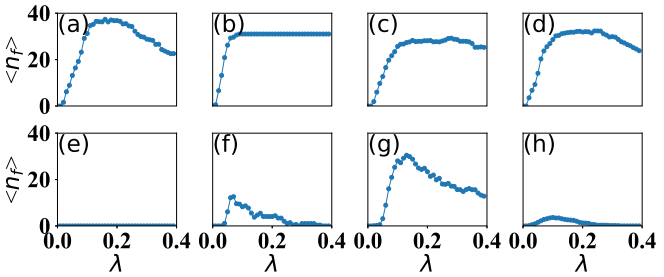

FIG. 5. Firing propagation on the eight cognitive networks where $\langle n_f \rangle$ represents the average of n_f on every source node of network. Panels (a)–(h) represent the dependence of $\langle n_f \rangle$ on λ for the cases of Att, Aud, CP, FP, mDm, MS, VT, and V systems, respectively.

visual network. Figures 4(d) and 4(e) show the dependence of n_f on the chosen source node i and the coupling λ for the ventral network, respectively, with $\lambda = 0.1$ in (d) and the source node 24 in (e). By comparing Fig. 4(d) with Fig. 4(a), we observe that there is more successfully firing propagation in (d) than in (a), suggesting that firing propagation also depends on the topologies of cognitive networks. Comparing Fig. 4(e) with Fig. 4(b), we see that the coupling range of firing propagation in Fig. 4(e) is much less than that in Fig. 4(b), confirming the dependence of firing propagation on the network topologies. Similarly, Fig. 4(f) shows the phase diagram of n_f on the phase plane of the source node i and the coupling strength λ for the ventral network. Comparing Fig. 4(f) with Fig. 4(c), we see that the successfully propagated region in Fig. 4(f) is much larger than that in Fig. 4(c), confirming again the influence of network topologies.

To illustrate how the topologies of cognitive networks influence firing propagation, we let each node i of network be the source node for one time and measure its $n_f(i)$. Then we let $\langle n_f \rangle$ be the average of $n_f(i)$ on every source node of network, i.e., $\langle n_f \rangle = \frac{1}{N}\sum_{i=1}^{N} n_f(i)$. Thus, $\langle n_f \rangle$ measures the average firing propagation of a cognitive network and will reflect the influence of network topology. Figures 5(a)–5(h) show the results for all the eight cognitive networks of Fig. 1, respectively. We see that they are significantly different from each other, i.e., $\langle n_f \rangle$ is relatively large in Figs. 5(a)–5(d) and 5(g), small in Figs. 5(f) and 5(h), but even zero in Fig. 5(e). We will figure out their mechanisms in Sec. IV.

B. Remote firing propagation in cognitive networks of human brain with one source node

All the above results belong to the case of normal firing propagation in cognitive networks. It will be of special interest if we can go beyond, such as studying the possibility of RFP. This problem is important as it can help us to understand how brain functions emerge from brain structural networks. Fortunately, in numerical simulations, we do observe the phenomenon of RFP in cognitive networks of human brain with one source node. Take the ventral network as an example. Figure 6 shows two typical pathways of RFP in the ventral network with a single source node, where the "red" and "gray" circles represent the firing nodes and inactivated nodes, respectively, and Fig. 6(a) represents the case with the source node 63 and coupling strength $\lambda = 0.38$ and Fig. 6(b) the

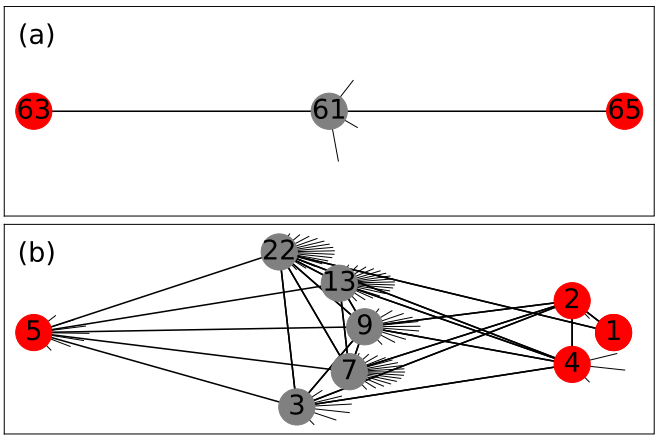

FIG. 6. Two typical pathways of RFP in a ventral network by one source node, where the "red" and "gray" circles represent the firing nodes and inactivated nodes, respectively. Panel (a) represents the case of a single driven relay node, with the source node 63 and coupling strength $\lambda = 0.38$. Panel (b) represents the case of multiple driven relay nodes, with the source node 5 and coupling strength $\lambda = 0.13$.

case with the source node 5 and coupling strength $\lambda = 0.13$. We see from Fig. 6(a) that the remote firing node ins 65 is connected only to the inactivated intermediate node 61, implying that the inactivated node 61 is a single driven relay node. In Fig. 6(b) there are three remote firing nodes, the nodes 2, 4, and 1, and five inactivated intermediate nodes, the nodes 3, 7, 9, 13, and 22, indicating that the inactivated nodes 3, 7, 9, 13, and 22 are multiple driven relay nodes.

Figure 6 shows only the dynamics of the ventral network along the pathways of RFP but does not account for the dynamics of all the other nodes. To show the dynamics of all nodes, an alternative way is to make a topological transformation of the network as follows. We let the source node i be the center, its nearest neighbors be the first circle, the nearest neighbors' neighbors be the second circle, and so on. In this way we can clearly show the dynamics of all nodes. Figure 7(a) shows the results of Fig. 6(b) where the "red" and

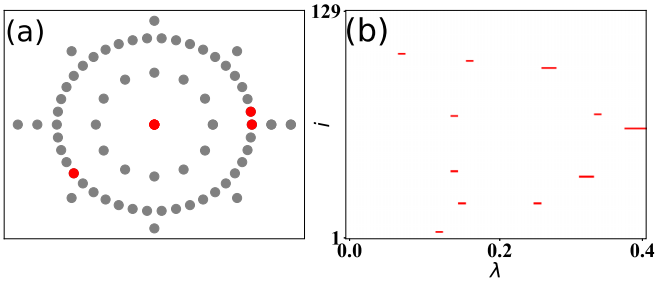

FIG. 7. RFP with only one source node. (a) Dynamics of all the nodes of ventral network for the case of Fig. 6(b), i.e. with the source node 5 and coupling strength $\lambda = 0.13$, where the "red" and "gray" points represent the firing and inactivated states, respectively. The center represents the source node and the first circle represents its nearest-neighboring nodes and so on. (b) Dependence of RFP on the source node i and the coupling strength λ where the "red" points represent the regions of RFP in the phase diagram.

"gray" points represent the firing nodes and inactivated nodes, respectively. It is observed that there are no firing nodes on the first circle, but three firing nodes appear on the second circle. This indicates that these three firing nodes are the only activated nodes of RFP by the source node 5 at a coupling strength $\lambda = 0.13$, i.e., $n_f = 3$.

Based on Fig. 7(a), we can conveniently recognize the nodes of RFP from the source node i at a given coupling strength λ. In this way, Fig. 7(b) shows the phase diagram of RFP in the phase plane of the source node i and the coupling strength λ where the "red" points represent the regions of RFP. We see that the regions of RFP are sparsely distributed in the phase plane, indicating that there are some strict conditions for RFP to appear. We will discuss it in Sec. IV.

C. Firing propagation in cognitive networks of human brain with multiple source nodes

Now we move to the case of multiple source nodes. We take the case of two source nodes as an example, but the obtained results can be extended to more source nodes. Specifically, we randomly choose a pair of source nodes i and j and let them be the source nodes; that is, only the pair of source nodes i and j satisfy Eq. (2) while all the other nodes will be represented by Eq. (1). Then we count the number of activated nodes $n_f(i, j)$ in the whole network. We find that similar to Fig. 4, the value of $n_f(i, j)$ depends on both the source nodes i and j and the coupling strength λ. On the other hand, to reflect the influence of network topology, we make 800 different realizations by randomly choosing different pairs of source nodes i and j and then calculate their average $\langle n_f \rangle$. Figure 8 shows the results where Figs. 8(a)–8(h) represent the dependence of $\langle n_f \rangle$ on λ for the cases of Att, Aud, CP, FP, mDm, MS, VT, and V networks, respectively. Comparing Fig. 8(a)–8(h) with Figs. 5(a)–5(h), i.e., the case of only one source node, we see that for each corresponding panel between them, the value of $\langle n_f \rangle$ in Fig. 8 is larger than that in Fig. 5, indicating that the case of multiple source nodes favors firing propagation.

In particular, we observe a substantial difference between Fig. 8(e) and Fig. 5(e) where the former has a small but nonzero $\langle n_f \rangle$ while the latter has a zero $\langle n_f \rangle$. Similarly, the relatively smaller values of $\langle n_f \rangle$ in Figs. 5(f) and 5(h) have been largely increased in Figs. 8(f) and 8(h) and reach the

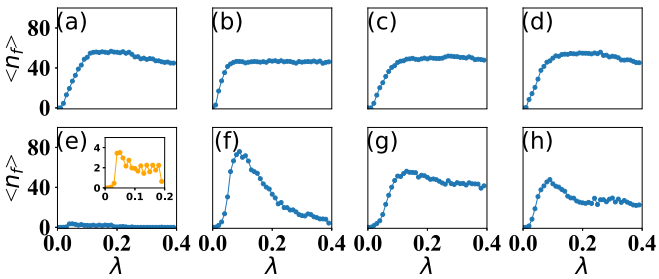

FIG. 8. Firing propagation of the eight cognitive networks for two source nodes where $\langle n_f \rangle$ represents the average of $n_f(i, j)$ on randomly chosen 800 pairs of source nodes i and j. Panels (a)–(h) represent the dependence of $\langle n_f \rangle$ on λ for the cases of Att, Aud, CP, FP, mDm, MS, VT, and V systems, respectively.

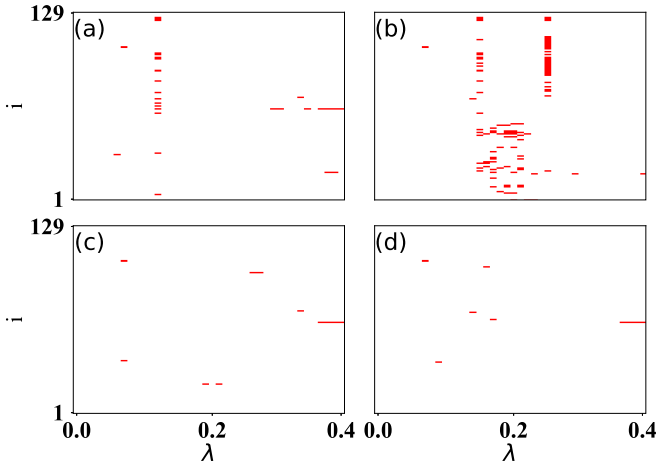

FIG. 9. Phase diagrams of RFP for two source nodes in ventral network, with the first source node being fixed as node j and the second source node going through all the other nodes. Panels (a) and (b) represent two typical cases for taking the first source node from the regions of RFP in Fig. 7(b), with $j = 5$ in (a) and $j = 21$ in (b). Panels (c) and (d) represent two typical cases for taking the first source node from outside of the regions of RFP in Fig. 7(b), with $j = 11$ (c) and $j = 35$ (d).

same level of Fig. 8(g), confirming again that the case of multiple source nodes favors firing propagation.

D. Remote firing propagation in cognitive networks of human brain with multiple source nodes

Based on the results of Fig. 8, we wonder whether multiple source nodes can also enhance RFP. To figure out the answer, we take the case of two source nodes as an example. For simplicity, we will fix one source node and then let the second source node go through all the other nodes. During this process, we will focus only on those nodes of RFP but ignore the nodes with normal firing propagation, i.e., the same way as in Fig. 7(b). In numerical simulations, we take the ventral network as an example. Figure 9 shows four typical cases where Figs. 9(a) and 9(b) represent the case that the first source node is chosen from the regions of RFP in Fig. 7(b), and Figs. 9(c) and 9(d) represent the case that the first source node is chosen from outside of the regions of RFP in Fig. 7(b). We see that all the four panels of Fig. 9 have regions of RFP, but the density in Fig. 9(a) and 9(b) is larger than that in Figs. 9(c) and 9(d).

Furthermore, it is important to compare Fig. 9 with two source nodes with Fig. 7(b) with one source node. This comparison reveals a striking difference: the densities in Fig. 9(a) and 9(b) are higher than those in Fig. 7(b), whereas the densities in Fig. 9(c) and 9(d) are lower, indicating two contrasting outcomes. We will figure out its mechanism in Sec. IV.

IV. THEORETICAL ANALYSIS ON BOTH THE FIRING PROPAGATION AND RFP

In this section we aim to give a brief theoretical explanation of the above observed firing propagation and RFP.

A. Case of normal firing propagation

We begin by discussing the case of firing propagation. In this case, we have observed the following results: (i) For a specific source node i, the number of activated nodes $n_f(i)$ depends on both the source node i and the coupling strength λ, i.e., $n_f(i)$ will be greater than zero only when the local topology of the source node i allows its activation to be propagated out and the coupling strength λ is located in the optimal range; see Fig. 4. (ii) For a cognitive network, its firing propagation $\langle n_f \rangle$ depends on the network topology; see Fig. 5. Finally, (iii) multiple source nodes favor firing propagation; see Fig. 8.

To understand the first aspect (i), we revisit Figs. 3(a) and 3(b), with firing propagation in Fig. 3(a) and no firing propagation in Fig. 3(b). A common point between them is that their numbers of the nearest neighbors of source nodes are approximately the same, i.e., the number of nodes on the first circle of the source node is $k_{80} = 15$ in Fig. 3(a) and $k_{11} = 12$ in Fig. 3(b). A key difference in their local topologies lies in the second circle: the number of nodes in the second circle is significantly smaller in Fig. 3(a) compared to Fig. 3(b). This suggests that the neighboring nodes of the first circle in Fig. 3(a) are fewer than those in Fig. 3(b). Thus, the ability of firing to propagate from the source node i to its first circle depends not only on the source node i and its nearest-neighboring nodes but also on the nodes of the second circle, i.e., the nearest neighbors' neighboring nodes of the source node i. This generates a deeper question: Why the higher degrees of the nodes on the first circle do not favor firing propagation. To figure out the answer, we go back to Eq. (1) and let

$$I_{\text{coup}} = \lambda \Sigma_{j=1}^{N} W_{mj}(x_j - x_m), \tag{3}$$

where m represents the nodes on the first circle of the source node i. Then we divide I_{coup} into two parts, $I_{\text{coup}} = I_1 + I_2$, with $I_1 = \lambda W_{mi}(x_i - x_m)$ from the source node i and $I_2 = \lambda \Sigma_{j=1, j\neq i}^{N} W_{mj}(x_j - x_m)$ from the second circle of the source node i. When the source node i is firing, we have $I_1 > 0$ as $x_i > x_m$. At this moment, we will generally have $x_j - x_m < 0$ and thus $I_2 < 0$; that is, I_1 will provide a positive contribution to I_{coup} while I_2 will provide a negative contribution to I_{coup}. When x_i is firing and x_j is not firing, we will have $x_i \gg x_j$, which makes the difference $x_i - x_m$ from the source node i balance the sum of several differences $x_j - x_m$ from the second circle of the source node i, resulting in $I_1 > |I_2|$ or $I_{\text{coup}} > 0$. In this case, node m on the first circle of the source node i will be activated, provided that we have $I_{\text{ext}} + I_{\text{coup}} > I_{\text{ext}}^c$ in Eq. (1). However, with the increase of the nodes on the second circle of the source node i, i.e., the increase of degrees of the nodes on the first circle, the balance between I_1 and I_2 will be broken, resulting in $I_1 < |I_2|$ or $I_{\text{coup}} < 0$. In this case, the node m on the first circle of the source node i will not be activated. This explains the observations in Figs. 3(a) and 3(b): $I_{\text{ext}} + I_{\text{coup}} > I_{\text{ext}}^c$ in Fig. 3(a) and $I_{\text{ext}} + I_{\text{coup}} < I_{\text{ext}}^c$ in Fig. 3(b). To provide evidence to support this analysis, we go back to Figs. 3(a) and 3(b) and show the degrees k_m of their nodes on the first circle of the source node i and other related information in Tables I and II, respectively, such as the connections within the first circle k_m^{in}, the connections to the second circle k_m^{out}, and the total weight to the second

TABLE I. Information on the nodes of the first circle of the source node i with $i = 80$ and degree $k_{80} = 15$ in Fig. 3(a) where the neighbor m, k_m, k_m^{in}, k_m^{out}, W_m^{out} and firing status represent the node number of the nearest neighbors of the source node 80, its corresponding degree, connections within the first circle, connections to the second circle, total weight to the second circle, and whether the node m is firing or not, respectively.

Source i	Neighbor m	k_m	k_m^{in}	k_m^{out}	W_m^{out}	Firing status
80	70	37	11	25	11.66	No
80	71	18	9	8	4.13	Yes
80	72	17	10	6	3.00	Yes
80	73	10	8	1	0.54	Yes
80	75	13	10	2	1.18	Yes
80	76	14	11	2	0.86	Yes
80	77	12	10	1	0.34	Yes
80	78	18	12	5	2.61	Yes
80	79	15	13	1	0.34	Yes
80	81	17	12	4	1.89	Yes
80	82	20	11	8	3.68	Yes
80	83	12	11	0	0	Yes
80	84	8	7	0	0	Yes
80	85	11	10	0	0	Yes
80	86	6	5	0	0	Yes

circle, which are extracted from Fig. 1(h) and Fig. 2(h), with $k_m^{\text{in}} + k_m^{\text{out}} = k_m - 1$.

We see from Tables I and II that most nodes on the first cycle for the firing status of "yes" do have smaller degree k_m and those for the firing status of "no" do have larger degree k_m, confirming the above analysis. More precisely, we see that the nodes of firing status of "no" have more connections to the second circle, k_m^{out}, implying that k_m^{out} plays a critical role in k_m. Going back to Eq. (3), we see that the weight W_{mj} represents the effective connection and thus is a better variable than k_m^{out} to represent the firing status. Let $W_m^{\text{out}} = \sum_{j=1}^{k_m^{\text{out}}} W_{mj}$.

TABLE II. Information on the nodes of the first circle of the source node i with $i = 11$ and degree $k_{11} = 12$ in Fig. 3(b) where the neighbor m, k_m, k_m^{in}, k_m^{out}, W_m^{out} and firing status represent the node number of the nearest neighbors of the source node 11, its corresponding degree, connections within the first circle, connections to the second circle, total weight to the second circle, and whether the node m is firing or not, respectively.

Source i	Neighbor m	k_m	k_m^{in}	k_m^{out}	W_m^{out}	Firing status
11	8	33	8	24	11.92	No
11	10	36	9	26	14.04	No
11	14	13	2	10	5.06	No
11	17	17	2	14	7.70	No
11	20	21	8	12	6.25	No
11	30	12	6	5	2.35	No
11	34	14	4	9	4.33	No
11	47	21	8	12	6.23	No
11	48	35	8	26	13.66	No
11	56	39	9	29	14.70	No
11	109	48	5	42	22.74	No
11	110	51	5	45	23.96	No

From Tables I and II, we see that W_m^{out} is indeed relatively large for the firing status of "no," indicating that it is the best quantity to represent firing propagation.

Based on the above analysis, we may come to an interesting conclusion that the peripheral nodes of a network favor firing propagation while the hub nodes do not, as the former usually have smaller degrees while the latter have larger degrees. After understanding these points, we can now easily explain the observation of Fig. 4(a), i.e. a key factor for $n_f > 0$ is its smaller W_m^{out}. Moreover, comparing Fig. 4(a) with Fig. 2(h), we see that the two peaks with $n_f > 0$ in Fig. 4(a) correspond to the two valleys with smaller degrees k_i in Fig. 2(h), confirming the above analysis again.

Furthermore, we can also apply Eq. (3) to explain the inactivated source nodes in Fig. 4(a). For the source nodes, we have $I_1 = 0$ and $I_2 < 0$, thus $I_{\text{coup}} = I_2 < 0$. Recall that the source node has an external stimulus I_s; see Eq. (2). Thus, the condition for the source node to fire is $I_{\text{ext}} + I_s + I_{\text{coup}} > I_{\text{ext}}^c$. Because of the existence of I_s, it is relatively easy for a source node to fire. However, when $|I_2|$ is large enough or there are enough nodes on the first circle of the source node, we will have $I_{\text{ext}} + I_s + I_{\text{coup}} < I_{\text{ext}}^c$. Once this happens, even the source node will not be activated. This is the reason for the "black" points on the x axis of Fig. 4(a).

Except the local topology of source node, another important factor for firing propagation is the coupling strength λ; see Figs. 4(c) and 4(f). It is well known that the key role of coupling is to make a synchronization among oscillators. This feature will definitely change the membrane potential x_i and thus change the difference $(x_j - x_m)$ in Eq. (3), i.e., influence the balance between $I_{\text{ext}} + I_{\text{coup}}$ and I_{ext}^c. When λ is too large, all the oscillators will be synchronized and thus result in $(x_j - x_m) = 0$, i.e., $I_{\text{coup}} = 0$. In this situation, we will have $I_{\text{ext}} + I_{\text{coup}} = I_{\text{ext}} < I_{\text{ext}}^c$ and thus no firing, confirming the observations in Figs. 4(c) and 4(f). Similarly, when λ is too small, we will have a very small I_{coup} from Eq. (3), also resulting in $I_{\text{ext}} + I_{\text{coup}} < I_{\text{ext}}^c$ and thus no firing in Fig. 4(c) and 4(f).

However, when λ is a middle value, its influence will depend on the local topology of the source node. Take the nodes on the first circle of the source node as an example. They will get the same positive contribution from the source node but different negative contribution from the connections to the second circle. At the same time, they will also interact each other through the connections within the first circle, i.e., k_m^{in}. These interactions from k_m^{in} will most probably result in a phase synchronization among the nodes on the first circle of the source node. To confirm it, Fig. 10 shows the dynamics of the nodes on the first circle of the source node for the case of Fig. 3, where Figs. 10(a) and 10(b) correspond to the cases of Figs. 3(a) and 3(b), respectively. We see that both Figs. 10(a) and 10(b) show phase synchronized behaviors, no matter they are firing or inactivated. In sum, the two aspects of the local topology of source node and coupling strength work together to make the firing propagation.

To understand the second aspect (ii), we go back to Fig. 2. We observe that all the panels in Figs. 2(a)–2(d) and Figs. 2(f) and 2(g) have a smaller average degree around 15–20, with smaller fluctuations, while the two panels of Figs. 2(e) and 2(h) have a larger average degree around 30, accompanied

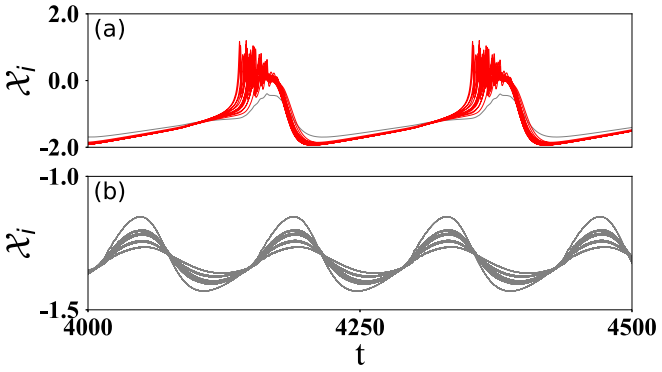

FIG. 10. Dynamics of the nodes on the first circle of the source node for the case of Fig. 3 where (a) and (b) correspond to the cases of Figs. 3(a) and 3(b), respectively.

by larger fluctuations. Based on this feature of topology, we deduce that the nodes on the first circle of the source node have relatively smaller degrees for the cognitive networks of Figs. 2(a)–2(d) and Figs. 2(f) and 2(g) but relatively larger degrees for the cognitive networks of Figs. 2(e) and 2(h); that is, it is relatively easier for the former to satisfy the condition of $I_{\text{coup}} > 0$ but difficult for the latter to satisfy the condition of $I_{\text{coup}} > 0$. This is the reason why we have observed larger firing propagation in the cognitive networks of Figs. 5(a)–5(d) and Figs. 5(f) and 5(g) but smaller firing propagation in the cognitive networks of Figs. 5(e) and 5(h).

To understand the third aspect (iii), we also go to the analysis of I_{coup}. In this case we have two source nodes and thus two first circles of the source nodes, resulting in more firing propagation. At the same time, the influence of the two source nodes may overlap at those subcritical nodes and make them reach the condition of $I_{\text{coup}} > 0$, resulting in the enhanced firing propagation in Fig. 8.

B. Case of remote firing propagation

We next discuss the case of RFP. In this context, we have also observed three key aspects: (i) There are different pathways for RFP, as shown in Fig. 6(a) and 6(b). (ii) RFP depends on both the source node i and the coupling strength λ, as demonstrated in Fig. 7(b). (iii) Multiple source nodes may either enhance or reduce firing propagation, as seen in Fig. 9. To understand the first aspect (i), we take the pathway of Fig. 6(a) as an example. Figure 11(a) shows its dynamics with $\lambda = 0.38$ where the "red," "gray," and "blue" lines represent the dynamics of the source node 63, the nearest-neighboring node 61 of the source node 63, and the remote firing node 65, respectively. The source node 63 is a peripheral node of the ventral network, with only one link, and thus receives the minimum influence from other nodes of the ventral network. In this sense, its total synaptic current will be approximately $I_{\text{ext}} + I_s = 3.0$ from Eq. (2). To understand what $I_{\text{ext}} + I_s$ represents, we plot a bifurcation diagram of a single HR neuron in Fig. 11(c), i.e., $\lambda = 0$ in Eq. (1). We see that the single HR neuron will be located in the bursting region when $I_{\text{ext}} = 3.0$ in Fig. 11(c). This is the reason why we observe the bursting

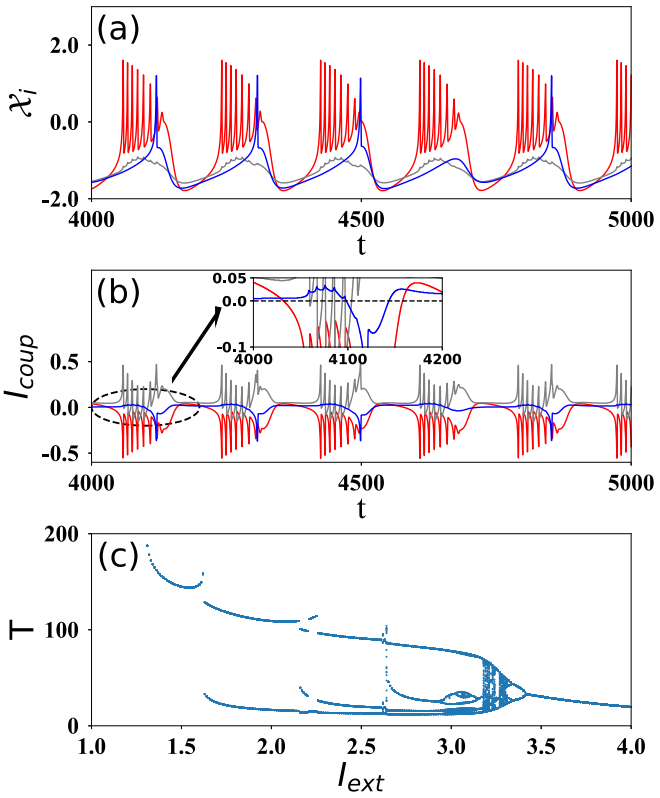

FIG. 11. Theoretical analysis on RFP. Panel (a) represents the dynamical process of RFP in Fig. 6(a) with $\lambda = 0.38$ where the "red," "gray," and "blue" lines represent the dynamics of the source node 63, the nearest-neighboring node 61 of the source node 63, and the remote firing node 65, respectively. Panel (b) represents the evolution of coupling term I_{coup}, corresponding to (a), where the inset shows the amplification of local dynamics. Panel (c) represents the bifurcation diagram of a single neuron of Eq. (1) with $\lambda = 0$.

behavior of the source node 63 in Fig. 11(a), i.e., the "red" line.

To understand the mechanism of the remote firing node 65, we show the behavior of I_{coup} in Fig. 11(b). We aim to provide evidence why the nearest-neighboring node 61 of the source node 63 is not activated but the remote node 65 is activated. As the "blue" line of the remote node 65 is too small to recognize, we amplify it in the inset. We see from the inset of Fig. 11(b) that the "blue" line of I_{coup} is greater than 0.01 right before the spike of node 65, resulting in $I_{\text{ext}} + I_{\text{coup}} > I_{\text{ext}}^c$ and thus inducing the spiking of remote firing node 65 in Fig. 11(a). More evidence is that the firing period of the remote firing node 65 is approximately 180, which is consistent with the period $T \approx 180$ for $I_{\text{ext}} = 1.31$ in Fig. 11(c). To further understand why the nearest-neighboring node 61 of the source node is not activated, we focus on the "gray" line in Fig. 11(b). We see that it is a fast oscillatory line, and thus its accumulated effect will cancel each other and lead to the subthreshold x_i in Fig. 11(a), i.e., no firing.

To understand the second aspect (ii), i.e., the influence of both the source node i and coupling strength λ, we take the pathway of Fig. 6(b) as an example. Figure 12(a) shows its dynamics where the "red," "gray," and "blue" lines represent the dynamics of the source node 5, the five nearest-neighboring

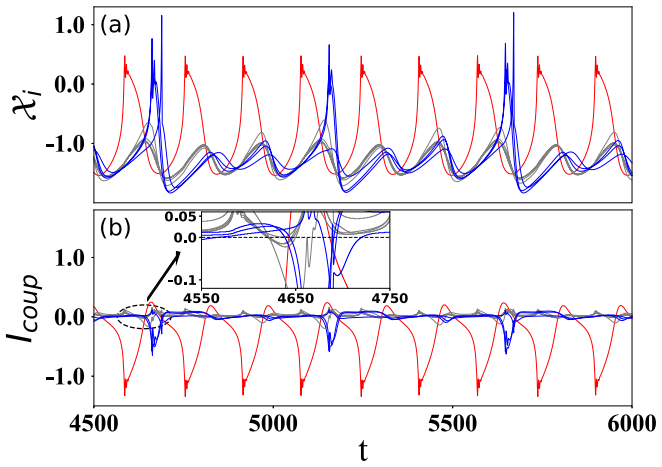

FIG. 12. Mechanisms of RFP in ventral network. (a) Dynamical process of RFP in Fig. 6(b) with $\lambda = 0.13$ where the "red," "gray," and "blue" lines represent the dynamics of the source node 5, the nearest-neighboring nodes 3, 7, 9, 13, and 22 of the source node 5, and the remote firing nodes 1, 2, and 4, respectively. (b) Evolution of I_{coup}, corresponding to (a).

nodes 3, 7, 9, 13, and 22 of the source node 5, and the three remote firing nodes 1, 2, and 4, respectively. To understand the mechanism of the three remote firing nodes 1, 2, and 4, we also show their corresponding I_{coup} in Fig. 12(b). From the inset of Fig. 12(b), we see $I_{\text{coup}} > 0.01$ and thus satisfy the condition of $I_{\text{ext}} + I_{\text{coup}} > I_{\text{ext}}^{c}$, resulting in the remote firing of the nodes 1,2, and 4. Comparing Fig. 12(a) with Fig. 11(a), we see that they are distinctively different, i.e., a burst in Fig. 11(a) but a spike in Fig. 12(a), reflecting the different influences of their source nodes. On the other hand, we notice that the source node 63 of Fig. 11(a) is a burst while the source node 5 of Fig. 12(a) is a spike. To understand this difference, we go back to Figs. 6(a) and 6(b). A distinctive difference between them is that the degree of the source node is $k_{63} = 1$ in Fig. 6(a) and $k_5 = 12 > 5$ in Fig. 6(b); that is, for Fig. 6(b), the source node 5 will also get influence from other parts of ventral network. As this influence depends on λ, it reflects the impact of coupling strength and causes $I_{\text{ext}} + I_s + I_{\text{coup}}$ of Eq. (2) to shift from the bursting region to the spiking region.

For the third aspect (iii), i.e. the influence of multiple source nodes, we have shown that the firing densities in Figs. 9(a) and 9(b) are larger than those in Fig. 7(b), while the firing densities in Figs. 9(c) and 9(d) are smaller than those in Fig. 7(b). To understand these two contrary results, we first need to distinguish between the nodes of RFP in Fig. 7(b) and those of normal firing propagation. Generally, a RFP will emerge only when the normal firing propagation is impossible; that is, there will be no possibility for RFP when firings can be normally propagated. In this sense, RFP can be considered as complementary of normal firing propagation. Then we go back to the case of two source nodes. When the first source node can make RFP, the second source node will help the regions of RFP to increase and thus enhance RFP. However, when the first source node has no RFP, it usually has a possibility of normal firing propagation. In this sense, the second source node will help the regions of normal firing propagation to increase and thus reduce the chance for RFP. These are what we have observed in Fig. 9(a)–9(d).

V. DISCUSSIONS AND CONCLUSIONS

From our work, some insights on signal propagation in cognitive networks can be summarized as follows. (i) RFP is a specific feature of network, which cannot be generated in a one-dimensional chain. Based on this feature, we may expect a spontaneous firing even without the source node. For example, when a node is in the critical point and fortunately gets a positive contribution from its neighbors, it might be activated. (ii) Peripheral nodes in the network favor firing propagation, in contrast to the conventional view that hub nodes are more crucial than peripheral nodes. This finding may induce clinical improvements to prevent the rapid spread of epilepsy or other disorders. Finally, (iii) the community topology of cognitive networks prefers local firing propagation and thus supports the diversity of brain functions.

Firing propagation and RFP reflect how information is regulated in cognitive networks and thus can be considered as a window to understand the mechanisms of the "black box," i.e., the way the brain works. In this sense, the study of firing propagation and RFP can help us understand how brain functions emerge from structural networks, providing a complementary and alternative perspective to remote synchronization. We also note that we selected source nodes at random to illustrate the firing propagation for several plots in this analysis. However, this does not influence our conclusions, as they are based on the condition that every node of a network is chosen as the source node for one time, indicating the robustness of source nodes. From the obtained phase diagrams of Figs. 4, 7, and 9, we can explore applications such as strategically choosing source nodes to achieve certain firing propagation. For example, depending on the requirement for propagation, we can use these phase diagrams to guide our choice of source nodes.

Finally, we must emphasize that all the results discussed above are based solely on negative feedback couplings. In the real brain, there are also inhibitory connections that will undoubtedly affect signal propagations. We leave this for future studies.

In conclusion, we have studied firing propagation in all eight cognitive networks of a brain network. We find that firing propagation can be significantly influenced by both the global topology of the network and the local topology of the source node. In particular, peripheral nodes of a network usually have a stronger ability of firing propagation than hub nodes. There is an optimal coupling strength related to synchronization for each cognitive network, and multiple source nodes favor firing propagation. Interestingly, a phenomenon of RFP is observed, which highlights the advantage of the network, in contrast to the case of a one-dimensional chain. Furthermore, a detailed theoretical analysis is provided to explain both the firing propagation and RFP.

ACKNOWLEDGMENTS

This work was partially supported by STI2030-Major Projects 2021ZD0202600 and the NNSF of China under Grants No. 12175070 and No. 42461144209.

[1] M. Breakspear, Dynamic models of large-scale brain activity, Nat. Neurosci. **20**, 340 (2017).

[2] A. Fornito, A. Zalesky, and M. Breakspear, The connectomics of brain disorders, Nat. Rev. Neurosci. **16**, 159 (2015).

[3] E. Bullmore and O. Sporns, Complex brain networks: Graph theoretical analysis of structural and functional systems, Nat. Rev. Neurosci. **10**, 186 (2009).

[4] S. N. Dorogovtsev, A. V. Goltsev, and J. F. F. Mendes, Critical phenomena in complex networks, Rev. Mod. Phys. **80**, 1275 (2008).

[5] F. Battiston, G. Cencetti, I. Iacopini, V. Latora, M. Lucas, A. Patania, J. Young, and G. Petri, Networks beyond pairwise interactions: Structure and dynamics, Phys. Rep. **874**, 1 (2020).

[6] D. Ghosh, M. Frasca, A. Rizzo, S. Majhi, S. Rakshit, K. Alfaro-Bittner, and S. Boccaletti, The synchronized dynamics of time-varying networks, Phys. Rep. **949**, 1 (2022).

[7] F. Crick and C. Koch, Some reflections on visual awareness, Cold Spring Harb. Symp. Quant. Biol. **55**, 953 (1990).

[8] D. G. Margineanu, Epileptic hypersynchrony revisited, Neuroreport **21**, 963 (2010).

[9] A. Pikovsky, M. Rosenblum, and J. Kurths, *Synchronization: A Universal Concept in Nonlinear Sciences* (Cambridge University Press, Cambridge, 2001).

[10] A. Arenas, A. Diaz-Guilera, J. Kurths, Y. Moreno, and C. Zhou, Synchronization in complex networks, Phys. Rep. **469**, 93 (2008).

[11] S. Boccaletti, J. A. Almendral, S. Guan, I. Leyva, Z. Liu, I. Sendiña-Nadal, and Y. Zou, Explosive transitions in complex networks' structure and dynamics: Percolation and synchronization, Phys. Rep. **660**, 1 (2016).

[12] M. J. Panaggio and D. M. Abrams, Chimera states: coexistence of coherence and incoherence in networks of coupled oscillators, Nonlinearity **28**, R67 (2015).

[13] Z. Wang and Z. Liu, A Brief review of chimera state in empirical brain networks, Front. Physiol. **11**, 724 (2020).

[14] T. Wu, X. Zhang, and Z. Liu, Understanding the mechanisms of brain functions from the angle of synchronization and complex network, Front. Phys. **17**, 31504 (2022).

[15] Z. Liu, Physical mechanisms of human brain functions, Quant. Biol. **13**, e70 (2025).

[16] N. C. Rattenborg, C. J. Amlaner, and S. L. Lima, Behavioral, neurophysiological and evolutionary perspectives on unihemispheric sleep, Neurosci. Biobehav. Rev. **24**, 817 (2000).

[17] N. C. Rattenborg, S. L. Lima, and C. J. Amlaner, Half-awake to the risk of predation, Nature (London) **397**, 397 (1999).

[18] M. Tamaki, J. W. Bang, T. Watanabe, and Y. Sasaki, Night watch in one brain hemisphere during sleep associated with the first-night effect in humans, Curr. Biol. **26**, 1190 (2016).

[19] J. A. Acebron, S. Lozano, and A. Arenas, Amplified signal response in scale-free networks by collaborative signaling, Phys. Rev. Lett. **99**, 128701 (2007).

[20] Z. Liu and T. Munakata, Scale-free topology induced double resonance in networked two-state systems, Phys. Rev. E **78**, 046111 (2008).

[21] T. Kondo, Z. Liu, and T. Munakata, One-body theory for amplified signal response in a scale-free network, Phys. Rev. E **81**, 041115 (2010).

[22] X. Liang, Cong Liu, and X. Zhang, Positive and negative couplings perform complementary roles in the signal amplification of globally coupled bistable oscillators, Phys. Rev. E **101**, 022205 (2020).

[23] L. Deng, S. Huo, A. Chen, and Z. Liu, Coupling resonance of signal responses induced by heterogeneously mixed positive and negative couplings in cognitive subnetworks, Chaos Solit. Fractals **180**, 114505 (2024).

[24] P. Ji, J. Ye, Y. Mu, W. Lin, Y. Tian, C. Hens, M. Perc, Y. Tang, J. Sun, and J. Kurths, Signal propagation in complex networks, Phys. Rep. **1017**, 1 (2023).

[25] U. Harush and B. Barzel, Dynamic patterns of information flow in complex networks, Nat. Commun. **8**, 2181 (2017).

[26] C. Hens, U. Harush, S. Haber, R. Cohen, and B. Barzel, Spatiotemporal signal propagation in complex networks, Nat. Phys. **15**, 403 (2019).

[27] X. Zhang, D. Witthaut, and M. Timme, Topological determinants of perturbation spreading in networks, Phys. Rev. Lett. **125**, 218301 (2020).

[28] K. D. Harris, Neural signatures of cell assembly organization, Nat. Rev. Neurosci. **6**, 399 (2005).

[29] Dynamic connetcome lab, https://www.dynamic-connectome.org.

[30] J. G. White, E. Southgate, J. N. Thomson, and S. Brenner, The structure of the nervous system of the nematode *Caenorhabditis elegans*, Philos. Trans. R. Soc. Lond. B **314**, 1 (1986).

[31] L. R. Varshney, B. L. Chen, E. Paniagua, D. H. Hall, and D. B. Chklovskii, Structural properties of the *Caenorhabditis elegans* neuronal network, PLoS Comput. Biol. **7**, e1001066 (2011).

[32] Q. Shen and Z. Liu, Remote firing propagation in the neural network of *C. elegans*, Phys. Rev. E **103**, 052414 (2021).

[33] Q. Shen and Z. Liu, Unidirectional links prefer local firing propagation in the neural network of *C. elegans*, Chaos Solit. Fractals **174**, 113850 (2023).

[34] Z. Wang and Z. Liu, Effect of remote signal propagation in an empirical brain network, Chaos **31**, 063126 (2021).

[35] Y. Qian, Z. Chen, R. Yang, H. Gao, Z. Lei, and Z. Zheng, Remote response modes on the paced excitable *C. elegans* network, Phys. Rev. Res. **6**, 033014 (2024).

[36] P. Hagmann, L. Cammoun, X. Gigandet, R. Meuli, C. J. Honey, J. V. Wedeen, and O. Sporns, Mapping the structural core of human cerebral cortex, PLoS Biol. **6**, e159 (2008).

[37] C. J. Honey, O. Sporns, L. Cammoun, X. Gigandet, J. P. Thiran, R. Meuli, and P. Hagmann, Predicting human resting-state functional connectivity from structural connectivity, Proc. Natl. Acad. Sci. USA **106**, 2035 (2009).

[38] L. Lord, A. B. Stevner, G. Deco, and M. L. Kringelbach, Understanding principles of integration and segregation using whole-brain computational connectomics: Implications for neuropsychiatric disorders, Phil. Trans. R. Soc. A **375**, 20160283 (2017).

[39] A. Avena-Koenigsberger, B. Misic, and O. Sporns, Communication dynamics in complex brain networks, Nat. Rev. Neurosci. **19**, 17 (2018).

[40] J. Wang, F. Lombardi, X. Zhang, C. Anaclet, and P. C. Ivanov, Non-equilibrium critical dynamics of bursts in θ and δ rhythms as fundamental characteristic of sleep and wake microarchitecture, PLoS Comp. Biol. **15**, e1007268 (2019).

[41] P. J. Uhlhaas and W. Singer, Abnormal neural oscillations and synchrony in schizophrenia, Nat. Rev. Neurosci. **11**, 100 (2010).

[42] S. Huo, C. Tian, M. Zheng, S. Guan, C. S. Zhou, and Z. Liu, Spatial multi-scaled chimera states of cerebral cortex network and its inherent structure-dynamics relationship in human brain, Natl. Sci. Rev. **8**, nwaa125 (2021).

[43] K. Bansal, J. O. Garcia, S. H. Tompson, T. Verstynen, J. M. Vettel, and S. F. Muldoon, Cognitive chimera states in human brain networks, Sci. Adv. **5**, eaau8535 (2019).

[44] D. Chen, Z. Yang, X. Liao, and Z. Liu, Heterogeneous network coupling induced 'local sleep'in brain cognitive networks, Nonlinear Dyn. **112**, 16409 (2024).

[45] H. R. Wilson and J. D. Cowan, Excitatory and inhibitory interactions in localized populations of model neurons, Biophys. J. **12**, 1 (1972).

[46] K. Bansal, J. D. Medaglia, D. S. Bassett, J. M. Vettel, and S. F. Muldoon, Data-driven brain network models differentiate variability across language tasks, PLoS Comput. Biol. **14**, e1006487 (2018).

[47] F. Wendling, J. J. Bellanger, F. Bartolomei, and P. Chauvel, Relevance of nonlinear lumped-parameter models in the analysis of depth-EEG epileptic signals, Biol. Cybern. **83**, 367 (2000).

[48] C. Zhou, L. Zemanova, G. Zamora-Lopez, C. C. Hilgetag, and J. Kurths, Structure–function relationship in complex brain networks expressed by hierarchical synchronization, New J. Phys. **9**, 178 (2007).

[49] S. Huo and Z. Liu, Condensation of eigenmodes in functional brain network and its correlation to chimera state, Commun. Phys. **6**, 285 (2023).

[50] M. Zheng, A. Allard, P. Hagmann, Y. Aleman-Gomez, and M. A. Serrano, Geometric renormalization unravels self-similarity of the multiscale human connectome, Proc. Natl. Acad. Sci. USA **117**, 20244 (2020).

[51] J. Hindmarsh and R. M. Rose, A model of neuronal bursting using three coupled first order differential equations, Proc. R. Soc. Lond. B **221**, 87 (1984).

[52] M. Dhamala, V. K. Jirsa, and M. Ding, Transitions to synchrony in coupled bursting neurons, Phys. Rev. Lett. **92**, 028101 (2004).